Engineering Structures 284 (2023) 115951

Contents lists available at ScienceDirect

Engineering Structures

journal homepage: www.elsevier.com/locate/engstruct

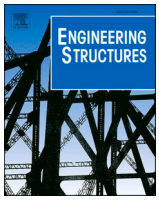

Shear behaviour of FRP-confined concrete/UHPC core-encased rebar: Experimental investigation and design method

Li Hu [a,b], Peng Feng [a,*], Jia-Qi Yang [c], Zhiyuan Li [a]

[a] Department of Civil Engineering, Tsinghua University, Beijing 100084, China
[b] Institute of Defense Engineering, AMS, PLA, Beijing 100085, China
[c] School of Mechanics and Civil Engineering, China University of Mining and Technology (Beijing), Beijing 100083, China

ARTICLE INFO

Keywords:
FRP tube
FCCC-R
Shear behaviour
UHPC

ABSTRACT

FRP-confined concrete/UHPC (ultra-high-performance concrete) core-encased rebar (FCCC-R) is a recently developed novel structural component for FRP-concrete composite structures. FCCC-R utilization can improve both the strength and ductility of composite structural members under both axial compression and combined bending-compression loading. When implemented in vertical structural members such as columns and shear walls with a low shear-span ratio, FCCC-Rs are subjected to combined axial compression and shear. In this study, the shear behaviour of FCCC-Rs is experimentally investigated. A total of 28 FCCC-R specimens are tested. The failure mechanism and modes, the load–deflection curves and the ultimate strength were obtained from the experiments. The FCCC-Rs exhibited higher load capacity and deformability. It could be concluded that the combination of the FRP tube, concrete and rebar can achieve the effect of "1+1+1>3". Furthermore, the influence of the shear-span ratio, concrete strength, tube thickness and fibre orientation are examined. Finally, design equations for the shear strength of FCCC-Rs are proposed, which attain a good agreement with the test data.

1. Introduction

As a linear elastic material with a relatively high rupture strain, fibre-reinforced polymers (FRPs) can provide passive confinement to concrete structural members under compression [1,2]. In particular, regarding passively confined concrete with a uniformly distributed lateral confining stress, e.g., FRP-confined circular columns under axial compression, the stress–strain curve can exhibit a bilinear response with a second ascending portion. Numerous theoretical models have been developed to describe and predict this kind of behaviour [1–4], and the mechanisms of both analysis- and design-oriented models were explicitly explained by Yang and Feng with a 3D geometrical approach [5–7]. Inspired by the behaviour of passively confined concrete, various FRP-concrete or FRP-steel–concrete composite structural members have been proposed by researchers [8–10]. In the early stage, concrete-filled FRP tubes (CFFTs) were developed [11], which can be directly employed as columns or piers. In CFFTs, filament-wound FRP tubes not only function as external confining materials but also function as moulds for concrete pouring, which is convenient for construction. FRP tubes can also protect the inner part of composite members from corrosion, making these tubes a viable solution for structures in aggressive environments, such as marine structures [12].

Although CFFTs attain an excellent performance under axial compression, the strength enhancement for eccentrically loaded CFFTs is limited, which is attributed to the nonuniformly distributed confining stress across the concrete section. To overcome this limitation, the authors' research group proposed composite column sections with concrete locally confined by CFFTs, i.e., the FRP-confined concrete/UHPC (ultra-high-performance concrete) core (FCCC) [8,9]. In terms of use, the CFFT as a column and the CFFT as an embedded reinforcement in a structural member (i.e. FCCC) are two different application forms of FRP confined concrete. The former works independently and the latter works with the encasing concrete and stirrups. In the composite section, FRP tubes are located in regions under high compressive stress to improve the confining efficiency (Fig. 1a). Based on the FCCC concept, the authors further developed the FRP-confined concrete core-encased rebar (FCCC-R), in which a high-strength steel bar is encased in the FCCC, as shown in Fig. 1b [13–15]. FCCC-R application provides two major advantages: (1) locally confined concrete can produce a bilinear response when subjected to compression, which can enhance the compressive

* Corresponding author.
E-mail address: fengpeng@tsinghua.edu.cn (P. Feng).

https://doi.org/10.1016/j.engstruct.2023.115951
Received 9 September 2022; Received in revised form 22 February 2023; Accepted 4 March 2023
Available online 20 March 2023

strength and ductility of the composite member; (2) FCCC-Rs can prevent longitudinal high-strength steel bars from premature buckling and can allow high-strength steel bars to reach the yield strength under extreme loading conditions such as earthquakes or sudden failure of adjacent structural members. Hence, this can reduce the possibility of progressive building collapse. Recent tests also confirmed the performance of RC shear walls embedded with FCCCs or FCCC-Rs [16,17]. With a proper arrangement of FCCC or FCCC-R components, the

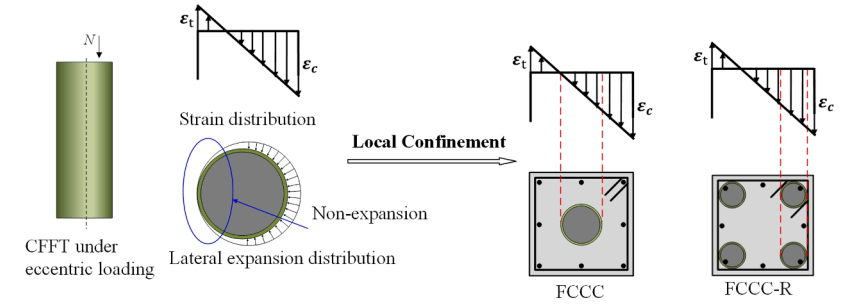

(a) Proposal of FCCC and FCCC-R to better use CFFTs under eccentric loading

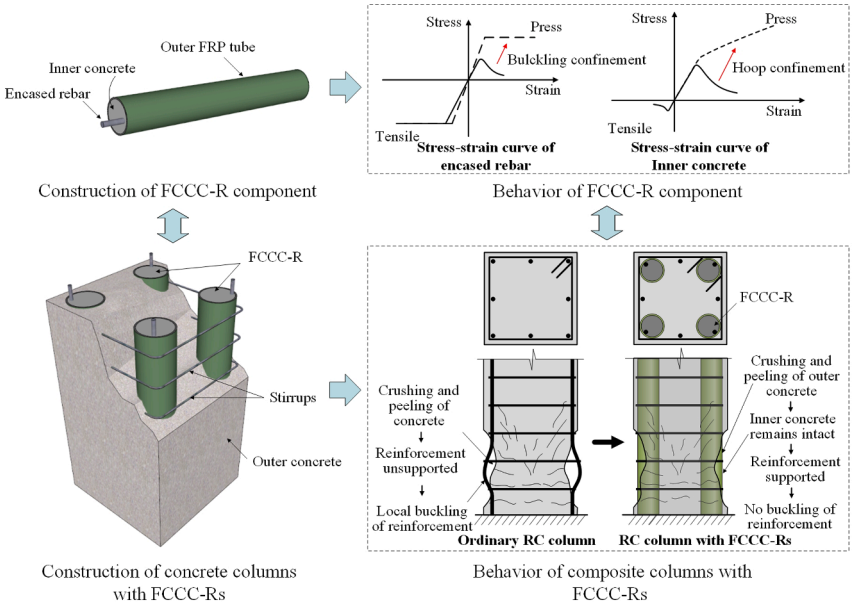

(b) Construction and behavior of composite columns with FCCC-Rs[]

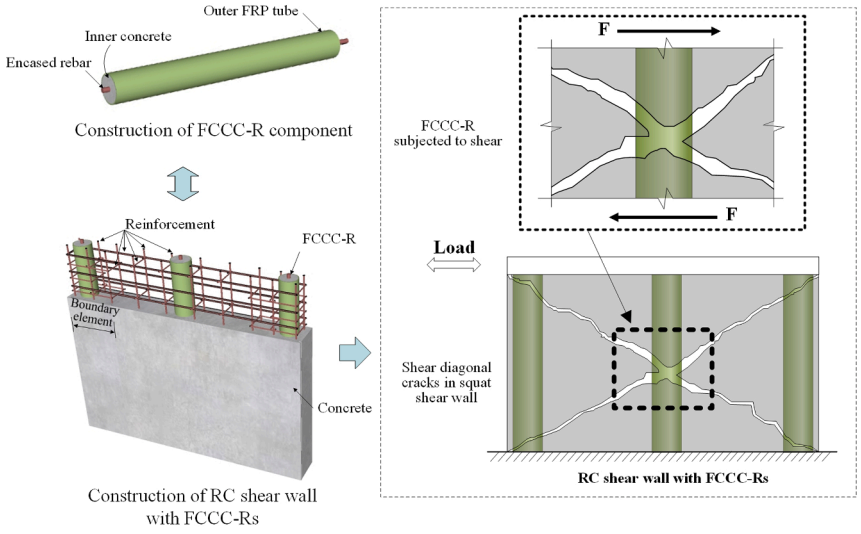

(c) Proposal of composite shear walls with FCCC-Rs

Fig. 1. Concept and development of the composite structural elements with FCCCs/FCCC-Rs.

ductility of the shear walls was enhanced up to 187 %. Previous studies also demonstrated that FCCC-R components are not only axially compressed but also subjected to shear (Fig. 1c) [16,17]. Therefore, it is of great importance to investigate the shear behaviour of FCCC-Rs to further develop a design method for composite structural members containing FCCC-Rs.

Existing studies are mainly concerned with the shear behaviour of CFFTs. Seible [18] proposed bridge pier retrofitting with CFFTs and derived equations for shear capacity prediction with a multi-component additive model similar to that for reinforced concrete members under cyclic shear loads. However, the model proposed by Seible neglected the bi-axial stress state and curvature [19]. Davol [20] and Burgueño [21] conducted scaled and full-scale CFFT four-point bending tests, respectively, and they analysed the deformation mode of CFFTs under shear load. Thereafter, Burgueño and Bhide [22–23] proposed analytical models for the shear load-deformation behaviour of CFFTs involving sectional-layered analysis. Ahmad [24] and Ahmad et al. [25] conducted bending tests of 10 short CFFT specimens and proposed analytical models based on strut-and-tie theory to predict the shear strength. This series of studies indicated that shear failure only occurs in specimens with a shear-span ratio lower than 1.0, and both the concrete strength and fibre orientation in FRP tubes can influence the load-bearing capacity of CFFT specimens. Therefore, with proper design, CFFTs can achieve optimal performance. Regarding CFFTs with longitudinal reinforcements, Fam and Cole [26] tested 14 steel- or FRP bar-reinforced CFFT specimens with shear-span ratios between 1.0 and 2.0 under monotonic bending loads, and the behaviours of reinforced CFFTs under cyclic flexural loads were studied by Shi et al. [27]. For the CFFT as a column, its length is generally much larger than its diameter. In other words, it works with a large shear-span ratio. Besides, it generally bears a heavy axial load and less shear load. Therefore, researchers showed limited concern about the CFFT's shear performance especially for the case that the shear-span ratio is lower than 1.0. However, when the CFFT is embeded in a column or shear wall, the shear action is localised at the shear crack reagion, leading to a quite low shear-span ratio. Therefore, studies of the shear behaviour of FCCC-Rs, especially with a shear-span ratio under 1.0 are necessary.

To bridge this research gap, 28 FCCC-R specimens were designed and tested in this study to investigate the shear behaviour of these novel structural components. The specimens were tested under three-point bending, and the influence of the shear-span ratio, concrete strength, tube thickness and fibre orientation were investigated. Finally, design equations for the shear strength of FCCC-Rs were proposed, which attained a good agreement with the test data.

2. Experimental setup

2.1. Details of the specimens

All the FRP tubes used for FCCC-R specimen casting have the same inner diameter, namely, 100 mm. A high-strength steel bar with a diameter of 18 mm is encased along the central axis of the FRP tube in each specimen. A test specimen is schematically shown in Fig. 2, where H denotes the length of the shear-span and D_0 denotes the inner diameter of the FRP tube.

There are 14 types of designed specimens with four variables investigated, i.e., shear-span ratio (λ), compressive strength of the infilling material (f_c), tube thickness (t) and fibre orientation (θ, which denotes the angle between the fibre direction and the tube axis). The shear-span ratio is calculated as $\lambda = H/D_0$ and is set to 1.0, 0.5 or 0.2 by varying the H value of the test specimens. Two types of ordinary concrete (strength grade C40/C60) and UHPC are designed as infilling materials for the FCCC-R specimens. Additionally, two thicknesses of the FRP tubes (t = 3 mm and t = 4 mm) are tested, and two types of fibre orientations (θ=±85° and θ=±60°) are investigated. The FRP tubes with fibre orientations of ± 60° have been widely-used in all kinds of scenarios and are the easiest to obtain. According to the studies of the CFFT columns, the CFFT adopting the FRP tube with the fibres aligned near the hoop direction exhibited better axial performance [7,28]. Therefore, the FRP tubes with these two fibre orientations were adopted. In addition, two types of CFFT specimens and a group of reinforced concrete cylinders without FRP tubes are tested as control specimens. There are two identical test specimens in each case. Details of the test specimens are listed in Table 1. The specimens are labelled as follows: T[*tube thickness*]A[*fibre orientation*]-[*concrete type*]R-[*shear-span ratio*]-[*specimen number*]. Regarding the tube thickness, T3 and T4 indicate t = 3 mm and t = 4 mm, respectively. In terms of the fibre orientation, A85 and A60 indicate θ values of ± 85° and ± 60°, respectively. For example, specimen T3A85-C40R-0.5-1 represents the first specimen with t = 3 mm, θ=±85°, concrete type C40, with an encased rebar and λ = 0.5. When the letter "R" is ommitted, it represents a CFFT without encased rebar.

2.2. Material properties

Two types of ordinary concrete and UHPC are employed as infilling materials for the FCCC-R specimens. The target cube strengths of C40 and C60 concrete are 40 MPa and 60 MPa, respectively, and the target strength of UHPC is 120 MPa. The ordinary concrete is ready-mix provided by a local supplier. UHPC is prepared from commercial mixed

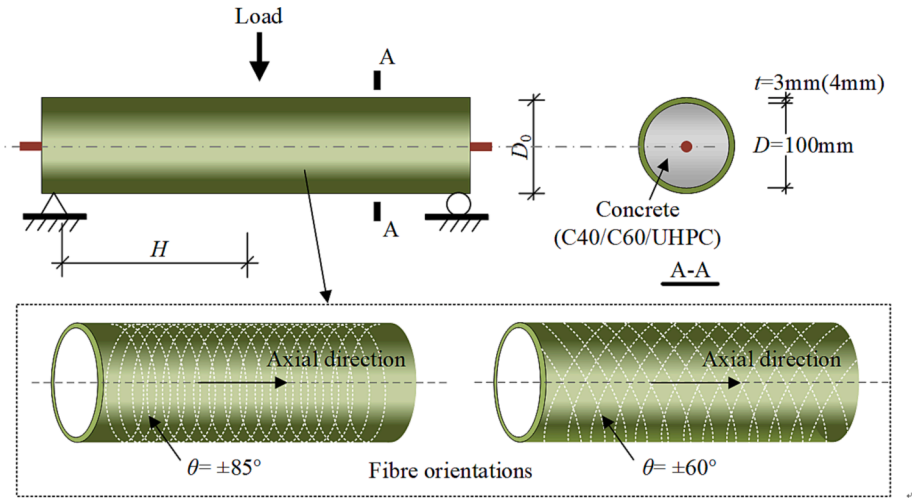

Fig. 2. Schematic diagram of a specimen.

Table 1
Specimen details.

Specimens	t (mm)	θ (°)	Concrete type	$\lambda(=H/D_0)$
T3A85-C40R-0.5	3	±85°	C40	0.5
T3A85-C60R-0.5	3	±85°	C60	0.5
T3A85-UHPCR-0.5	3	±85°	UHPC	0.5
T3A60-C60R-0.5	3	±60°	C60	0.5
T3A60-UHPCR-0.5	3	±60°	UHPC	0.5
T4A85-C60R-0.5	4	±85°	C60	0.5
T3A85-C60R-1	3	±85°	C60	1
T3A85-UHPCR-1	3	±85°	UHPC	1
T3A85-C60R-0.2	3	±85°	C60	0.2
T3A85-UHPCR-0.2	3	±85°	UHPC	0.2
T3A85-UHPC-0.5[a]	3	±85°	UHPC	0.5
C60R-0.5[b]			C60	0.5
UHPCR-0.5[b]			UHPC	0.5
UHPC-0.5[c]			UHPC	0.5

[a] Specimens without an encased rebar.
[b] Specimens without an FRP tube.
[c] Specimens without either an FRP tube or an encased rebar.

materials with a water-to-cement ratio of 0.18. The UHPC contains discrete steel fibres with a fibre volume of 1 %. The determined 150-mm cube strengths of C40 and C60 are 52.1 MPa and 64.5 MPa, respectively, and the determined 100-mm cube strength of UHPC is 125.6 MPa. With the determined cube strength, the compressive strength (f_c) is calculated according to Chinese code GB50010 [29,30] and Lv et al. [31], as listed in Table 2. The calculated material properties are adopted in analytical modelling. The encased high-strength steel bars of grade PSB830 exhibit a diameter of 18 mm. Three steel bar specimens are tested in tension, and the average yield strength and ultimate strength are 978 MPa and 1152 MPa, respectively.

The FRP tubes used in this study consist of 2400 tex E-glass fibres and epoxy resin. There are three types of tubes for specimen casting, including a tube with a winding angle of 60° with a nominal thickness of 3 mm, a tube with a winding angle of 85° with a nominal thickness of 3 mm, and a tube with a winding angle of 85° with a nominal thickness of 4 mm, i.e., T3A60, T3A85 and T4A85, respectively. The lateral strength and stiffness of these FRP tubes are obtained by splitting the disk test according to ASTM D2290-12 [32]. Detailed properties of the FRP tubes are reported in Table 3.

2.3. Test setup and instrumentation

All FCCC-R specimens are tested under symmetrical three-point bending. The test setup and instrumentation are shown in Fig. 3. The cylindrical specimens are simply supported by arch-shaped steel supporters. Arch-shaped supporters and loading plate have the same curvature with the FRP tube, which can increase the contact area and relieve the stress concentration significantly. The load is applied through an arch-shaped loading plate by a 3000 kN testing machine. It should be noted that H is the distance between the edge of the supporters and the loading plate. The loading rate is displacement controlled as 0.1 mm/min.

Five LVDTs are installed to measure the displacement of the specimens, as shown in Fig. 3, in which LVDT-1 measures the mid-span deflection, and LVDT-2 and LVDT-3 measure the deformation at the supports. LVDT-2 and LVDT-3 are affixed to extra shelves, ensuring that the measured displacement is the absolute displacement of the supporters. LVDT-4 and LVDT-5 measure the slip between the FRP tube and inner concrete with one end fixed to the concrete surface and the other end attached to the FRP tube. Eight strain gauges are uniformly distributed at the middle of one of the shear spans to measure the hoop strains of the FRP tube. Additionally, longitudinal and 45° inclined strain gauges are installed at the centre of both shear spans to obtain the principal strain of the FRP tube. The arrangement and labelling of the strain gauges are shown in Fig. 3.

Table 2
Concrete properties.

Type	Cube compressive strength f_{cu} (MPa)	Axial compressive strength f_c (MPa)
C40	52.1	39.6
C60	64.5	51.0
UHPC	125.6	110.5

Table 3
Properties of the FRP tubes.

Type	Thickness t (mm)	Inner diameter D (mm)	Fibre orientation	Hoop strength $f_{f,11}$ (MPa)	Hoop elastic modulus $E_{f,11}$ (GPa)
T3A60	3	100	±60°	434	24.2
T3A85	3	100	±85°	670	47.4
T4A85	4	100	±85°	670	47.4

3. Experimental results

3.1. Behaviours and failure modes

The shear force (V) versus mid-span deflection (δ) responses of the test specimens can be classified into three typical types, as shown in Fig. 4. All three types of V-δ curves contain an almost linear ascending portion in the beginning. In terms of the type 1 curves, brittle failure occurs after the peak load with a sudden loss of strength. Among the type 2 curves, there is a sudden drop in load after the peak point. However, V still increases with δ at a lower rate and finally gradually decreases. Regarding the type 3 curves, after the initial linear potion, the stiffness gradually decreases before reaching the maximum load, and the load then decreases slowly until extreme deformation occurs in the specimens. Among the three types of V-δ responses, type 1 indicates brittle failure, while types 2 and 3 indicate ductile failure.

The shear performance of the FCCC-Rs depends on the shear resistance of the concrete, the dowel action of the steel rebars and the shear resistance of the FRP tubes similar to that of stirrups but is not a simple superposition of these components. The above three shear resistance types are manifested at different levels of displacement. To explain the relationship between the shear performance of the FCCC-Rs and the contribution of each component, the failure process of the specimens is divided into four stages, as shown in Fig. 5. It should be noted that for the FCCC-R specimens, only the cracks of the FRP tube could be seen during the tests and the crack patterns of the internal concrete were observed after removing the external FRP tube after the tests. In the beginning, all materials remain elastic, and the load-deflection curves are linear. With increasing applied load, the sound of concrete cracking can be heard, and slip between the FRP and concrete can be observed via the installed LVDTs, but there is no obvious visual phenomenon. At this stage, the load increases almost linearly at a lower rate than that at the elastic stage. At stage three, cracks emerge on the FRP tubes, and the slope of the load-deflection curves decreases. The crack patterns on the FRP tubes are different depending on the layout of the specimens. Finally, the specimens achieve their peak strengths and subsequently fail in different modes. The presence of the steel bar alters the failure mode of conventional CFFTs. Compared to a CFFT specimen without a steel bar (S-2 in Ahmad [24], which fails under flexure, the considered FCCC-R specimen (T3A85-C60R-1 in this study) exhibits a combined shear and flexural failure mode. This occurs because the steel bar can increase both the bending and shear capacities. The shear-span ratios of these three types of beams are very low. Under the same loading conditions, a plain concrete beam with a very low shear-span ratio soon experiences diagonal compression failure after the emergence of shear cracks. Regarding reinforced concrete beams without an FRP tube, the steel rebar along the central axis of the cross-section delay crack development. However,

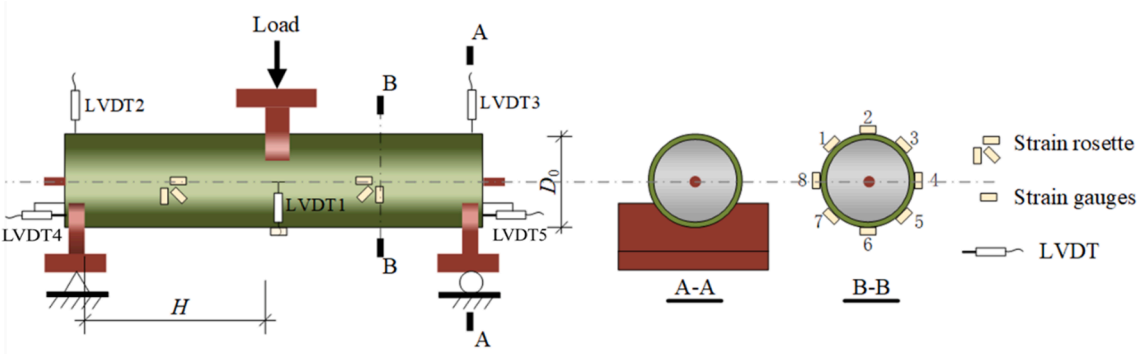

Fig. 3. Test setup and instrumentation.

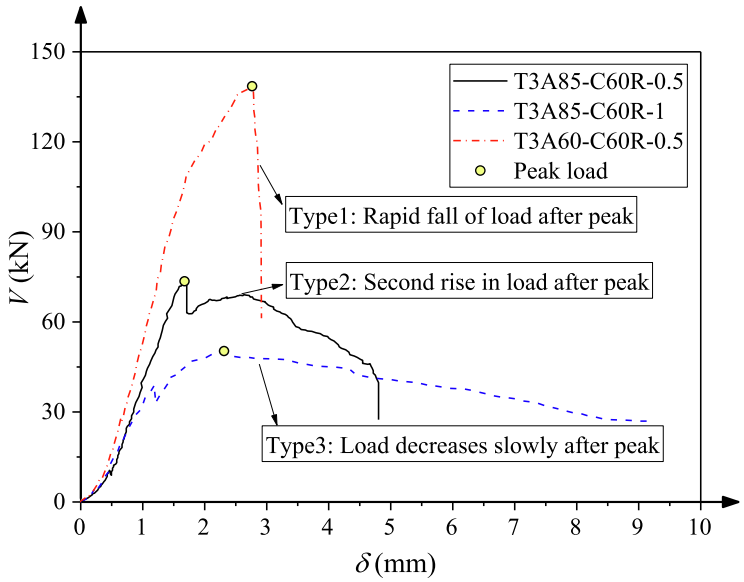

Fig. 4. Typical shear force (V) versus midspan deflection (δ) curves.

diagonal compression failure can still occur at the crack development stage. Among FCCC-Rs, since the external FRP tube plays a role similar to that of the stirrup, which can restrain crack propagation well and is more helpful to facilitate the dowel action of the embedded steel rebar, higher strength and greater mid-span deflection can be obtained. Obvious bending cracks and shear cracks can be observed when the FCCC-R specimens finally fail. Compared to an angle of ± 85°, the FCCC-R with a fibre winding angle of ± 60° attains a higher peak load because ± 60° is close to the direction vertical to the emerging diagonal cracks, and the FRP tube imposes a better inhibition effect on shear crack formation.

Fig. 6 shows the *V*–*δ* curves for all specimens. For most of the FCCC-R specimens (T3A85-UHPCR-0.5-2 in Fig. 6(c), T3A60-C60R-0.5 series in Fig. 6(d), C60R-0.5 series in Fig. 6(l), UHPCR-0.5-2 in Fig. 6(m), and UHPC-0.5 series in Fig. 6(n)), specimens with type 1 curves fail due to concrete shear failure. For this type of specimen, diagonal cracks propagate through the section at the peak load point, after which the composite action between the concrete and steel bar no longer occurs, and the load is only carried by the steel bar. Therefore, the type 1 curves exhibit a sudden loss of strength after the peak point. Specimens with type 2 curves (T3A85-C60R-0.5 series in Fig. 6(b), T3A85-UHPCR-0.5-1 in Fig. 6(c), T3A85-C60R-0.2 series in Fig. 6(i), T3A85-UHPCR-0.2-2 in Fig. 6(j), T4A85-C60R-0.5 series in Fig. 6(f), and T3A60-UHPCR-0.5 series in Fig. 6(e)) reveal combined shear and flexural failure modes, which are dominated by shear cracks. After reaching the first peak load point, diagonal cracks emerge on the specimens, but there remains a compression zone in the concrete section. Due to the dowel action of the steel bar, shear cracks stop propagating, and the load is carried by the bending action of the specimens. Therefore, the load decline after the first peak point indicates the transition of the load-bearing mode, and the following part of the curve captures the bending response of the specimen. Among the type 3 specimens (T3A85-C40R-0.5 series in Fig. 6(a), T3A85-C60R-1 series in Fig. 6(g), T3A85-UHPCR-1 series in Fig. 6(h), and T3A85-UHPCR-0.2-1 in Fig. 6(j)), both flexural and shear cracks can be observed on the concrete, and flexural cracks dominate the failure mode. Therefore, this type of specimen behaves similarly to RC flexural members.

It could be seen that there was an obvious difference for the two identical specimens in terms of stiffness, curve shape and failure modes. The specimens could roughly be divided into three types. Most of the testing results of the repeated specimens are similar, e.g. T3A85-C40R-0.5 in Fig. 6(a), T3A85-UHPCR-0.5 in Fig. 6(c). Some of the series in which the repeated specimens are different are related to inaccurate measurement caused by defects, e.g. T3A85-C60R-0.5 in Fig. 6(b), (d) T3A60-C60R-0.5 in Fig. 6(d). The specimens presented the same failure modes, and the shapes of the curves are similar, but their initial stiffnesses are different. This phenomenon was related to possible gaps between internal concrete and external FRP tubes in FCCC-Rs, and possible gaps between irregular surface of the FRP tubes and arch-shaped steel supporters or arch-shaped loading plate. The former was caused by shrinkage or poor casting quality of the internal concrete/UHPC and the latter was caused by nonuniform resin distributing during the

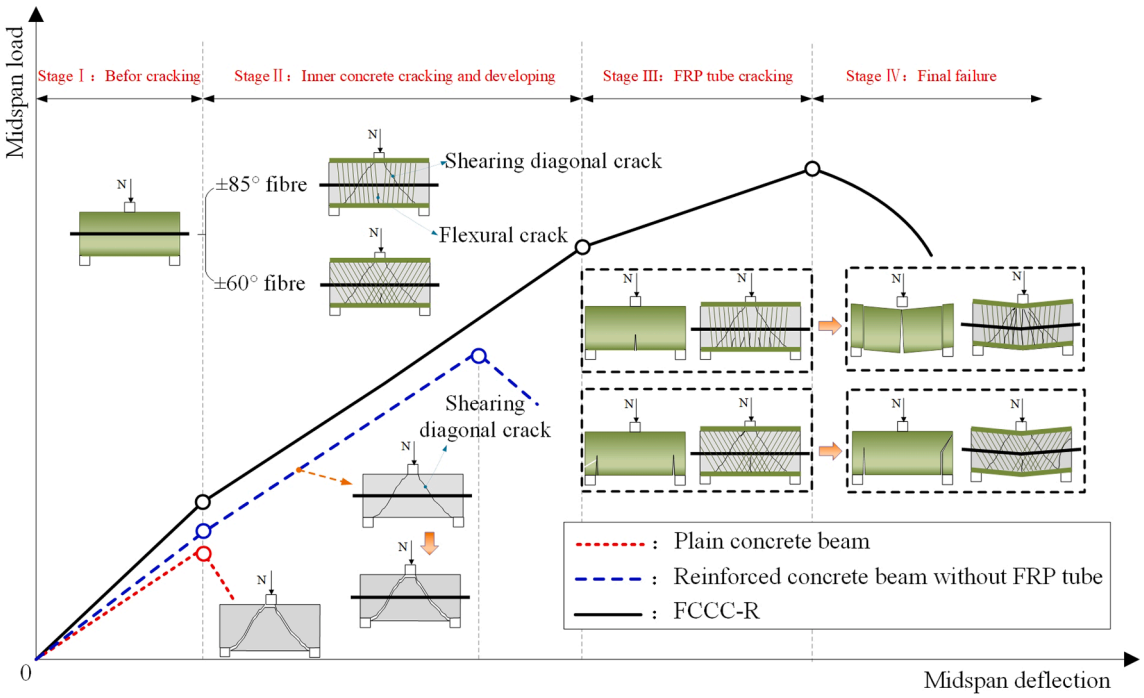

Fig. 5. Four stages of the failure process.

manufacturing process of the FRP tubes. In the beginning of the test, the gaps were closed gradually and the results of LVDTs included the deformation of the gaps and the shear/flexural deformation of the specimens and presented that there was obvious deformation. As the test processed, the gaps were fully closed and the results of LVDTs only included the shear/flexural deformation of the specimens and thus the deformation increased more slowly. These defects only appeared in some of specimens. Therefore, the curves of the specimens with these defects show an ascending branch with a low stiffness at the beginning and the stiffness increased gradually afterwards. Some of the series, e.g. T3A85-UHPCR-0.2 in Fig. 6(j), UHPCR-0.5 in Fig. 6(m), in which the repeated specimens are different are related to local poor casting quality of concrete. Materials in these areas failed prematurely, leading to the premature failure of the specimen. While, the repeated specimen didn't have such defects and behaved differently. Generally, these series were not utilized with the FRP tubes or the rebars. It could be concluded that, the combination effect of FRP tube, rebar and concrete can reduce the influence of the materials defects on the whole components.

After testing, FRP tubes were detached from the FCCC-R specimens, and three types of cracks were observed on the concrete surface, namely, flexural cracks (F), shear cracks (S), and local cracks near the supports (L), as shown in Fig. 7. These cracking types correspond to a specific cracking pattern which would happen in concrete beams under four-point bending test. Flexural cracks initiated in the middle span and propagated vertically, as shown in Fig. 7a. Shear cracks initiated at the supports and propagated towards the loading bear, which was always inclined to the specimen axis, as shown in Fig. 7b. Local cracks propagated vertically near the supports, which could be observed in the specimens with a low shear-span ratio, as shown in Fig. 7c. In fact, most of the specimens failed in the combined mode with at least two types of cracks, as shown in Fig. 7d. Failure modes were used to describe the cracking patterns which the specimens presented and could be some cracking type or the combination of the cracking types. The failure modes and curve types for all specimens are reported in Tables 4–7. Additionally, the maximum shear strength (V_e) and the corresponding mid-span deflection (δ_e) are listed in Tables 4–7 for each series of specimens.

Although arch-shaped supporters and loading plate were adopted to decrease the stress concentration in this test, the local compressive failure near the loading points and supports occurred for some specimens and largely affected the test results and the accuracy. This is because the modulus of the FRP tube and the steel supporters and loading plate are large. The local deformation of the FRP tube was distinct and that of the steel supporters and loading plate was less, which could lead to stress concentration. To relieve this problem, rubber gasket could be set between the FRP tube and the steel supporters and loading plate. Besides, the CFFT/FCCC-R could be embedded in concrete and the shear load was applied on the concrete, which is more similar with the FCCC-R in the structural member.

3.2. *Influence of the concrete strength*

The influence of the concrete strength (f_c) on the shear strength (V_e) is shown in Fig. 8a. Both individual (indv.) and average (Avr.) values are presented. The average shear strength (V_e) increases almost linearly with the strength of the infilling material (f_c) in the f_c series. In this series, λ is kept constant at 0.5, and all tubes are T3A85 tubes. The failure modes in this series are dominated by combined flexural and shear failure (F + S), and most of the specimens fail in the ductile mode (types 2 and 3), except for T3A85-UHPCR-0.5-2, with local cracks observed near the supported region.

3.3. *Influence of the shear-span ratio*

The influence of the shear-span ratio (λ) on the shear strength (V_e) is shown in Fig. 8b. Obviously, the shear capacities of the UHPC specimens are higher than those of the C60 specimens. With increasing λ, the dominant failure mechanism changes from shear to flexure. Therefore, V_e decreases for both types of specimens. Moreover, the results indicate greater dispersion when λ is low because the shear and local failure modes introduce more uncertainty. In addition, the shear properties of the UHPC specimens remain less consistent than those of the ordinary concrete specimens.

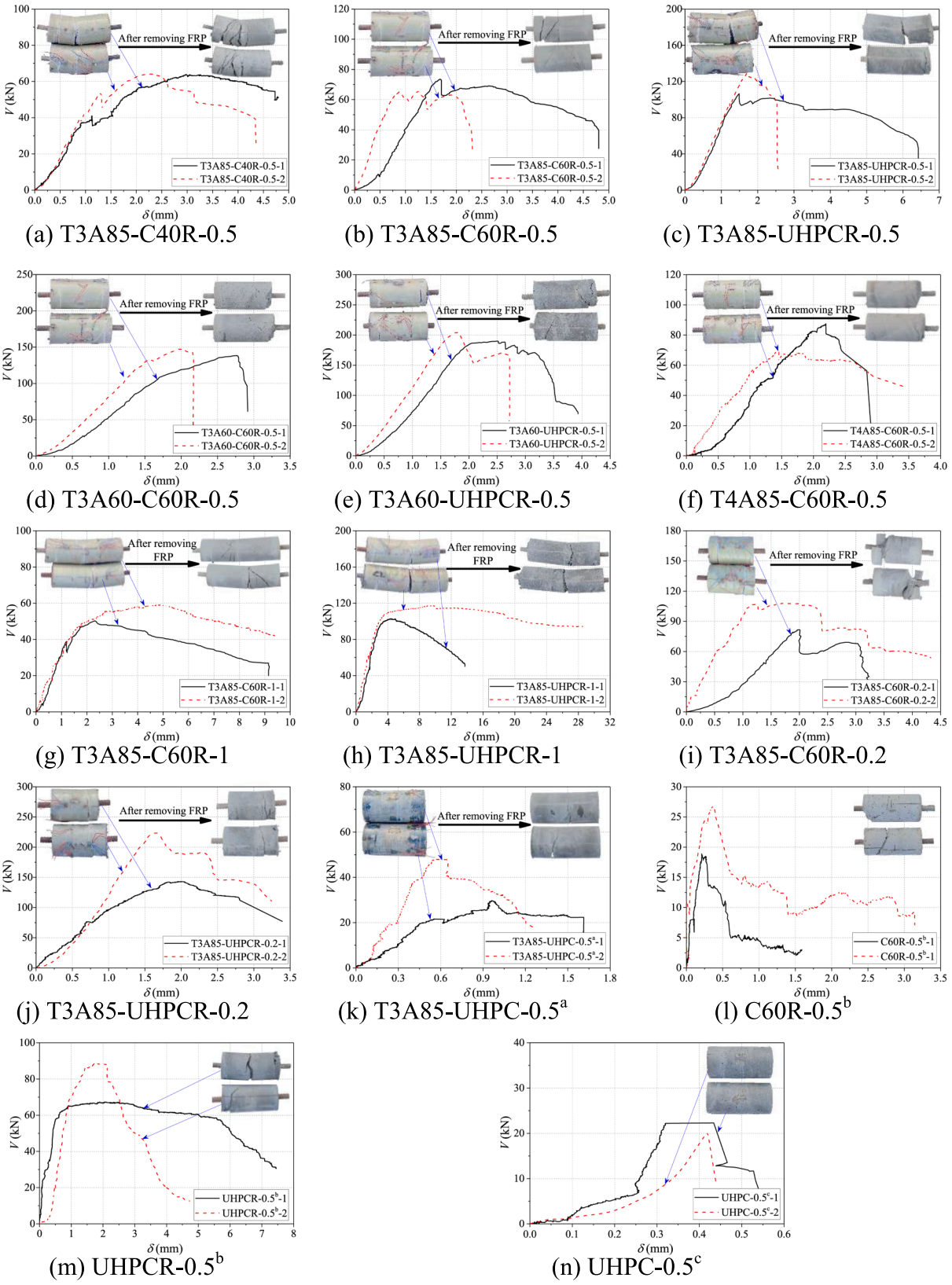

Fig. 6. Shear force (V) versus midspan deflection (δ) curves for all the specimens.

3.4. Influence of the FRP tubes

The test results for the t and θ series are shown in Fig. 8c and d, respectively. Apparently, a larger tube thickness can enhance the shear capacity of the FCCC-R specimens. Among the specimens with A85 tubes and $\lambda = 0.5$ filled with C60 concrete, the 3 mm and 4 mm tubes can enhance the shear strength to 204 % and 243 %, respectively, over the control specimens (C60R-0.5). Among the specimens filled with UHPC,

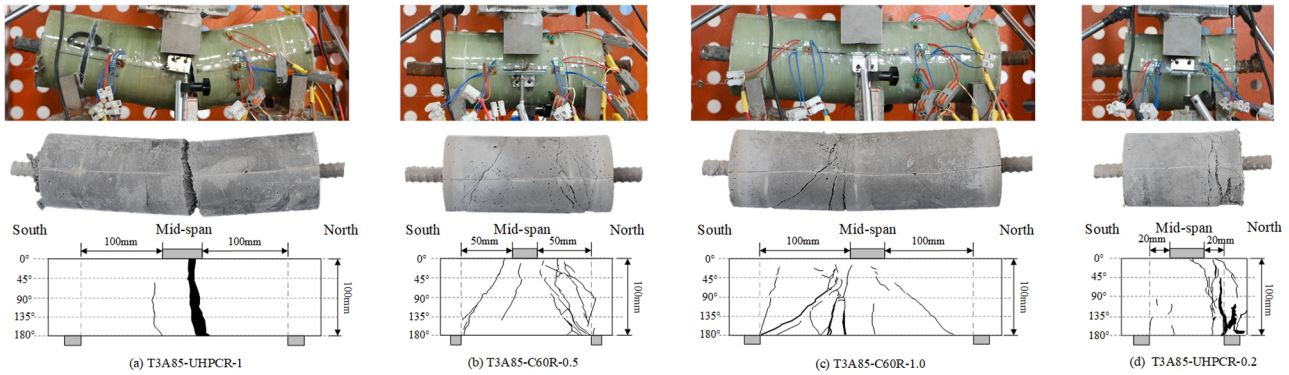

Fig. 7. Typical failure modes of the FCCC-R specimens.

Table 4
Test results for the f_c series.

ID	V_e[1](kN)	δ_e[2](mm)	Failure mode[3]	Curve type
T3A85-C40R-0.5-1	64	2.98	F + S	Type 3
T3A85-C40R-0.5-2	64	2.29	F + S	Type 3
Ave.[4]	64	2.63	/	
T3A85-C60R-0.5-1	74	1.68	F + S + L	Type 2
T3A85-C60R-0.5-2	66	1.25	S	Type 2
Ave.	70	1.46	/	
T3A85-UHPCR-0.5-1	106	1.49	F	Type 2
T3A85-UHPCR-0.5-2	129	1.73	F + S + L	Type 1
Ave.	118	1.61	/	

[1] V_e = shear strength;
[2] δ_e = midspan deflection corresponding to V_e;
[3] Failure modes: F = flexural cracking; S = shear cracking; L = local compressive failure at the supports;
[4] Ave. = average value of two identical specimens.

Table 5
Test results for the λ series.

ID	V_e^1(kN)	δ_e^2(mm)	Failure mode[3]	Curve type
T3A85-C60R-0.2-1	82	2.00	F + S	Type 2
T3A85-C60R-0.2-2	108	1.68	F + S	Type 2
Ave.[4]	95	1.84	/	
T3A85-C60R-0.5-1	74	1.68	F + S + L	Type 2
T3A85-C60R-0.5-2	66	1.25	S	Type 2
Ave.	70	1.46	/	
T3A85-C60R-1-1	50	2.31	F + S	Type 3
T3A85-C60R-1-2	60	4.89	F + S	Type 3
Ave.	55	3.60	/	
T3A85-UHPCR-0.2-1	143	1.95	S + L	Type 3
T3A85-UHPCR-0.2-2	220	1.68	S + L	Type 2
Ave.	182	1.81	/	
T3A85-UHPCR-0.5-1	106	1.49	F	Type 2
T3A85-UHPCR-0.5-2	129	1.73	F + S + L	Type 1
Ave.	118	1.61	/	
T3A85-UHPCR-1-1	103	4.30	F + S	Type 3
T3A85-UHPCR-1-2	117	9.56	F	Type 3
Ave.	110	6.93	/	

[1-4]Refer to the Table 4 footer.

Table 6
Test results for the t series.

ID	V_e^1(kN)	δ_e^2(mm)	Failure mode[3]	Curve type
C60R-0.5[b]-1	19	0.21	S + L	Type 1
C60R-0.5[b]-2	27	0.36	F + S	Type 1
Ave.[4]	23	0.28	/	
T3A85-C60R-0.5-1	74	1.68	F + S + L	Type 2
T3A85-C60R-0.5-2	66	1.25	S	Type 2
Ave.	70	1.46	/	
T4A85-C60R-0.5-1	88	2.19	S + L	Type 2
T4A85-C60R-0.5-2	70	1.46	S + L	Type 2
Ave.	79	1.82	/	
UHPCR-0.5[b]-1	67	1.89	F	Type 3
UHPCR-0.5[b]-2	89	1.77	S + L	Type 1
Ave.	78	1.83	/	
T3A85-UHPCR-0.5-1	106	1.49	F	Type 2
T3A85-UHPCR-0.5-2	129	1.73	F + S + L	Type 1
Ave.	118	1.61	/	
UHPC-0.5[c]-1	22	0.43	F	Type 1
UHPC-0.5[c]-2	20	0.42	F	Type 1
Ave.	21	0.43	/	
T3A85-UHPC-0.5-1	30	0.96	F	Type 3
T3A85-UHPC-0.5-2	48	0.56	S	Type 3
Ave.	39	0.76	/	

[1-4] Refer to the Table 4 footer.

Table 7
Test results for the θ series.

ID	V_e^1(kN)	δ_e^2(mm)	Failure mode[3]	Curve type
T3A85-C60R-0.5-1	74	1.68	F + S + L	Type 2
T3A85-C60R-0.5-2	66	1.25	S	Type 2
Ave.[4]	70	1.46		
T3A60-C60R-0.5-1	139	2.77	S + L	Type 1
T3A60-C60R-0.5-2	147	1.97	S + L	Type 1
Ave.	143	2.37		
T3A85-UHPCR-0.5-1	106	1.49	F	Type 2
T3A85-UHPCR-0.5-2	129	1.73	F + S + L	Type 1
Ave.	118	1.61		
T3A60-UHPCR-0.5-1	190	2.49	S + L	Type 2
T3A60-UHPCR-0.5-2	204	1.81	S + L	Type 2
Ave.	197	2.15		

[1-4] Refer to the Table 4 footer.

the 3-mm tube enhances the shear strength to 51 %. The contributions of the T3 tubes are 47 kN and 40 kN for the C60 and UHPC specimens, respectively, which are very similar. Therefore, in predicting the total shear strength of the FCCC-R specimens, it is reasonable to apply the superposition method to consider the contribution of the FRP tubes. Fibre orientation is another important factor influencing shear strength. As shown in Fig. 9, for most of the specimens, the results based on the strain rosette indicate that the direction of the principal strain on the shear-span is approximately 45° to the tube axis. Therefore, A60 tubes are more effective in shear resistance enhancement than A85 tubes. The increases in the shear strength for C60 and UHPC are 73 kN and 71 kN, respectively. Therefore, it can be inferred that the contribution of the FRP tubes can be considered separately from that of the infilling material, and the superposition method is applicable to this analysis.

The hoop strain distribution at the centre of the shear span for selected specimens is shown in Fig. 10, including specimens T3A85-UHPCR-0.5, T3A60-UHPCR-0.5, T3A85-C60R-0.2 and T3A85-C60R-1, which shows the influence of the fibre orientation of the FRP tubes and the shear-span ratio. As shown in Fig. 10, the hoop strains for all

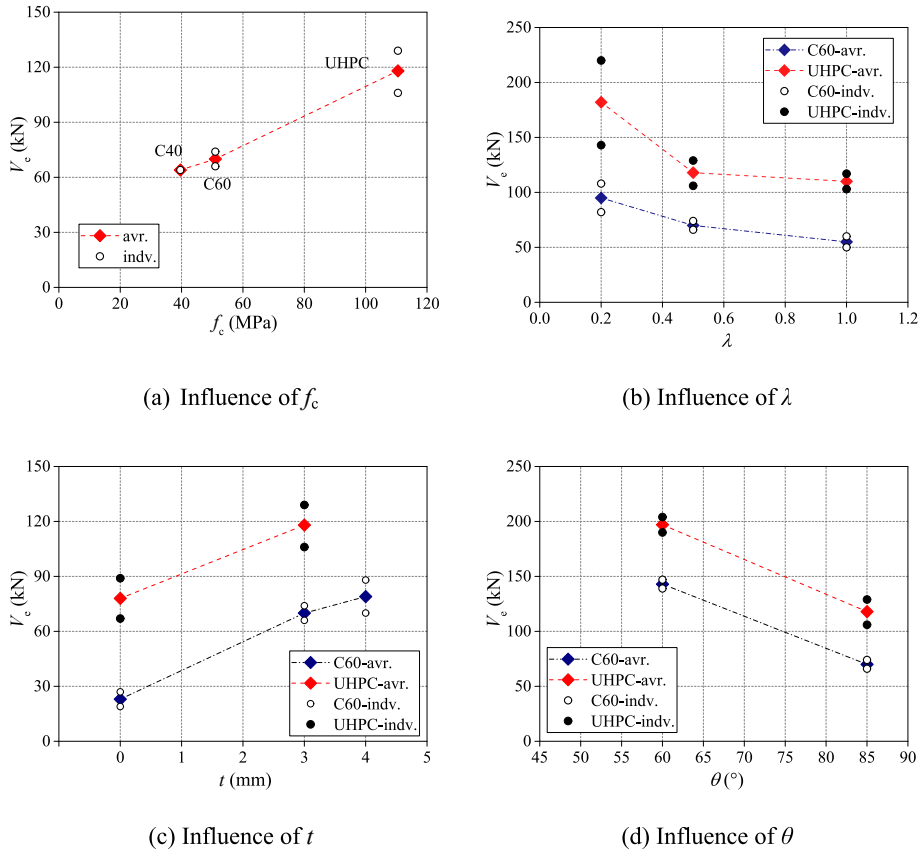

(a) Influence of f_c (b) Influence of λ

(c) Influence of t (d) Influence of θ

Fig. 8. Influence of different parameters.

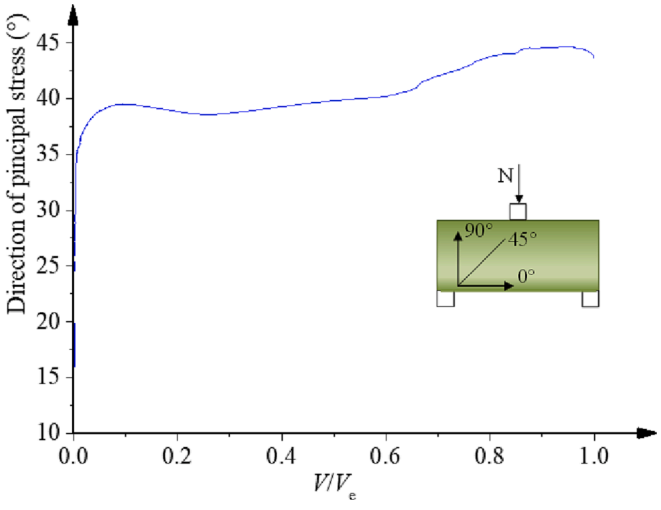

Fig. 9. Direction of the principal strain for specimen T3A85-UHPCR-0.2.

selected specimens are low, and the distribution is not uniform. This indicates that the confining effect of the FRP tubes is minor when FCCC-Rs are subjected to shear. The influence of the fibre orientation can be inferred by comparing Fig. 10a and b. The specimen with 60°-oriented fibres attains a lower and more uniformly distributed hoop strain because the inclined fibres can impede the opening of diagonal cracks. In contrast, the nonuniformity of the hoop strain distribution of the T3A85-C60R-0.5 specimen indicates that there occurs a diagonal crack propagating through the mid-shear-span section. It can be seen that the results from strain gauge 7# were larger, indicating that there was severe local deformation near strain gauges 7#. And thus, it could be speculated that there was also severe local deformation, i.e. cracks, near the concrete near strain gauge 7#. Strain gauge 7# lies in the 1/4 height of the cross-section and 1/4 span near the support (i.e. the mid-point between the support and the loading point). Generally, the cracks in this area are likely to be diagonal cracks. Hence, the 85°-oriented fibres are less effective in shear resistance enhancement, leading to severe diagonal cracks of internal concrete.

The influence of the shear-span ratio is shown in Fig. 10c and d. For the specimen T3A85-UHPCR-0.2, strain gauges 1# and 6# were significantly larger than others and the strain distributions were non-uniform. It could be speculated that there were severe diagonal cracks and the specimen suffered from shear failure, which agrees with the observation in Fig. 6i. For the T3A85-UHPCR-0.2 specimen, the strain distributions were more uniform than the specimens with less shear-span ratio and the strains were also less. It could be observed that the width of diagonal cracks was less. As shown in Fig. 6g, the specimens mainly failed in flexure or combined shear-flexure and the diagonal cracks were fewer. Generally, the conclusions from the strain gauges agreed with the failure modes observed in Section 3.1. As the shear-span ratio decreases, the diagonal cracks develop more.

When the shear-span ratio is low ($\lambda = 0.2$ in Fig. 10c), the concrete fails in shear (Fig. 6i). Therefore, the hoop strain is not uniform, and a severe strain concentration can be observed. When the shear-span ratio is higher ($\lambda = 1$ in Fig. 10d), the specimens mainly fail in flexure or combined shear-flexure. Thus, there are fewer diagonal cracks through the mid-shear-span section, and the hoop strains are low and uniformly distributed.

3.5. *Influence of the steel bar*

The presence of the steel bar changes the failure mode of conventional CFFT members. Due to the absence of a steel bar, the CFFT

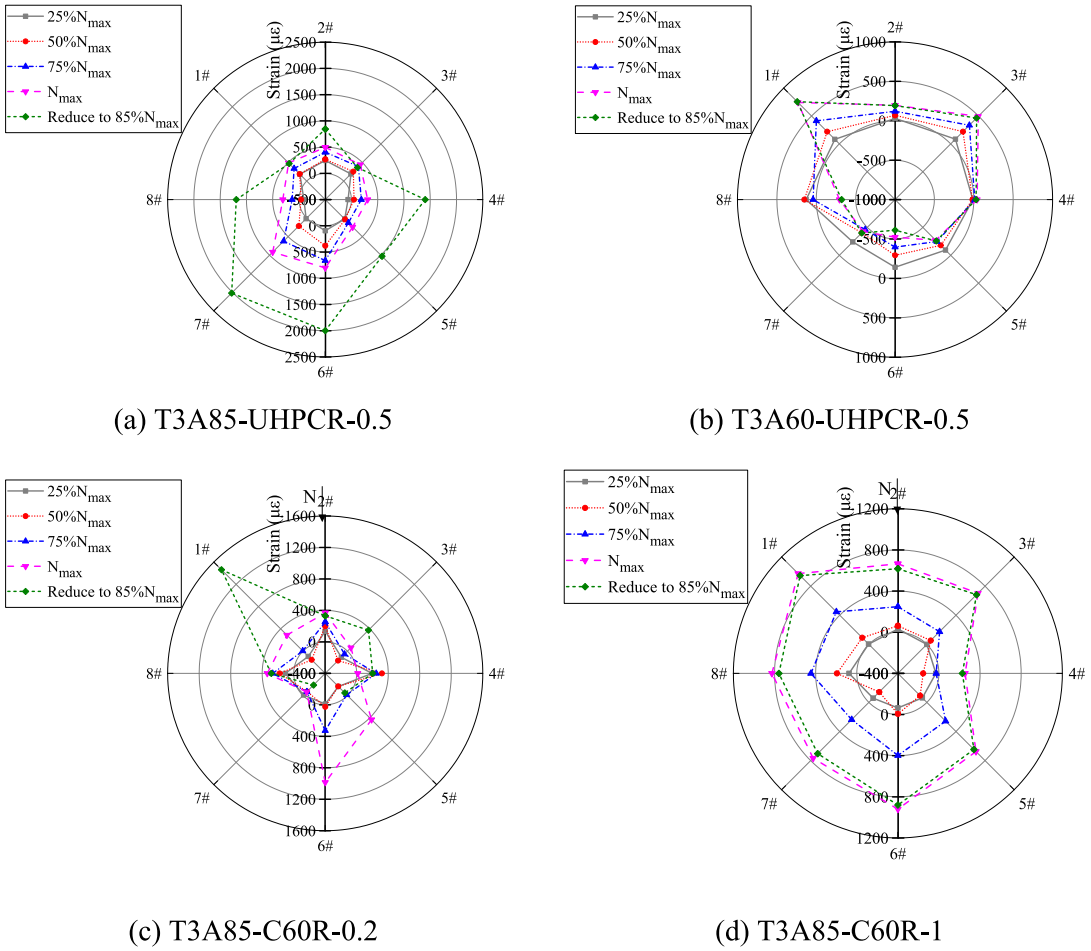

Fig. 10. Hoop strain of the middle section of the shear-span.

specimens always fail in the flexural mode even with a low shear-span ratio [24]. The encased steel bar can increase the flexural strength of the CFFT specimens. Hence, shear cracks form in the inner concrete during the test. In addition, the dowel action of the steel bar can improve the shear resistance. As indicated by the test results, the FCCC-R specimens always fail in the combined shear-flexure mode. Therefore, the presence of the steel bar can achieve a balanced shear-flexure effect.

The shear strengths of the specimens with encased steel bars are significantly higher than those without steel bars, despite the presence of FRP tubes. Choosing the specimens comprising UHPC as an example (shown in Fig. 11), the steel bars increase the average shear strength by 201 % and 271 %, and the contributions of the steel bars are 78 kN and 57 kN, respectively, for specimens with and without FRP tubes, respectively.

4. Design equations for the shear capacity of FCCC-Rs

The shear strength of FCCC-Rs is composed of three parts: (i) infilling material; (ii) encased steel bar; and (iii) shear resistance of the FRP tube. Most existing studies employ the superposition method to predict the shear strength of FCCCs, which is the summation of the contribution of each part. As mentioned earlier, the test results in this research also support this point of view. Therefore, the shear strength of FCCC-Rs can be written as:

$$V_{cal.} = V_c + V_f + V_s \quad (1)$$

where $V_{cal.}$ is the total shear strength of the FCCC-R, V_c is the shear strength of the infilling material (e.g., concrete or UHPC), V_f is the contribution of the FRP tube, and V_s is the contribution of the encased steel bar.

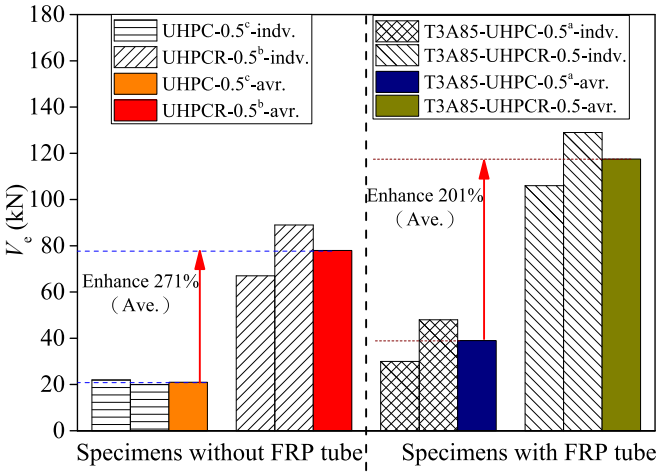

Fig. 11. Influence of the inner steel bar.

Bhide and Burgueño [22,23] proposed a strength model for CFFTs using the Euler-Bernoulli beam theory and a modified stress field. However, the basic assumption of this approach is that the strain is linearly distributed across the depth of the flexural specimen, which is not applicable in short beams, such as those with $\lambda \leq 1$. Other researchers, e.g., Ahmad [24], Ahmad and Zhu et al. [25] and Fam and Cole [26], proposed models based on the strut-and-tie model, which are

suitable for simulating the stress flow in a deep beam without steel stirrups. The following model was proposed by Ahmad [24]:

$$V_f = \sum_{i=1}^{n} \frac{\pi}{2} t_{fi} D_0 f_{\pm\alpha i} \tag{2}$$

where n is the total number of fibre layers, D_0 is the outer diameter of the tube, t_{fi} is the lamina thickness at the ith winding angle, and $f_{\pm\alpha i}$ is the ultimate tensile strength at winding angle α_i. In this study, however, the tubes are different from those used in Ahmad [24] in terms of the manufacturing technique, in which the layer thickness is difficult to obtain, and Eq. (2) does not consider the shear-span ratio (λ). Hence, this model cannot be directly adopted herein.

Based on the strut-and-tie model, Chinese code GB50608 [29,30] provides a design equation for the shear strength of FRP tubes in FRP-concrete composite structures:

$$V_f = \sum_{i=1}^{n} \frac{\pi}{2} t_{fi} E_{fi} \varepsilon_{fa} h (\sin\alpha_i + \cos\alpha_i)\sin\alpha_i \tag{3}$$

where E_{fi} is the nominal elastic modulus of the ith fibre layer, h is the diameter of the tube, α_i is the angle between the tube axis and fibre direction of the ith layer, and ε_{fa} is the allowed tensile strain of the fibres, which is 0.004. Based on the models reviewed above, the authors proposed a new shear strength model for the FRP tubes in FCCC-Rs in this study:

$$V_f = \frac{C_1}{\lambda + C_2} \pi t D f_{\pm\alpha} (C_3 \sin\alpha + C_4 \cos\alpha)\sin\alpha \tag{4}$$

where t is the total thickness of the FRP tube, D is the inner diameter of the FRP tube, $f_{\pm\alpha}$ is the uniaxial tensile strength of the FRP tube with a winding angle of $\pm\,\alpha$ degrees, and C_1, C_2, C_3 and C_4 are the parameters to be determined. Via regression of the test data, these four parameters are determined as 2.34, 0.3, 0.15 and 0.5, respectively.

The contribution of the infilling material V_c is determined with the Chinese code for concrete structures GB50010 [29,30]:

$$V_c = \frac{1.75}{\lambda + 1} \times 0.704 f_t D^2 \tag{5}$$

where f_t is the tensile strength of concrete, which can be calculated as $f_t = 0.395 f_{cu}^{0.55}$ [29,30], and f_{cu} is the cube strength of concrete. It should be noted that in Eq. (5), the range of λ should be $1.5 \le \lambda \le 3.0$.

The encased steel bar contributes to the shear strength mainly by the resultant dowel action. According to Vintzeleou and Tassios [33], the dowel action of steel bars can be calculated as:

$$V_s = 1.30 d_s^2 \sqrt{f_c f_y} \tag{6}$$

where d_s is the diameter of the steel bar, f_c is the compressive strength of the concrete, and f_y is the yield strength of the steel bar. The slippage between the concrete and steel bar decreases the contribution of the steel bar, which is more obvious for the FCCC-R specimens with a low shear-span ratio. Thus, according to the test data, a reduced coefficient ζ is proposed in this paper based on the experimental results.

$$\zeta = \frac{0.212}{\lambda + 0.66} \sqrt{f_c / 19.10} \tag{7}$$

where 19.10 is the design value of the axial compressive strength of C40 concrete, in MPa, and $\zeta = 1$ when the calculated value is greater than 1. For the FCCC-R specimens with a shear-span ratio not higher than 1.0, the shear strength provided by the dowel action can be calculated with Eq. (7).

$$V_{s,a} = \zeta V_s = \frac{0.276\sqrt{f_c/19.10}}{\lambda + 0.66} d_s^2 \sqrt{f_c f_y} \tag{8}$$

By substituting Eqs. (4), 5 and 8 into Eq. (1), the shear capacity of FCCC-Rs yields:

$$V_{cal.} = \frac{1.232}{\lambda + 1} f_t D^2 + \frac{2.34}{\lambda + 0.3} \pi t D f_{\pm\alpha} (0.15\sin\alpha + 0.5\cos\alpha)\sin\alpha + \frac{0.276\sqrt{f_c/19.10}}{\lambda + 0.66} d_s^2 \sqrt{f_c f_y} \tag{9}$$

With the use of Eq. (9), the shear capacity of all the specimens is calculated ($V_{cal.}$) and compared to the experimental results ($V_{exp.}$), as shown in Fig. 12. The mean value of the ratio of the predicted values to the test values is 1.00, with $R^2 = 0.97$. Fig. 12 indicates that the proposed equations fit the test data well and are conservative in high-strength regions, which is suitable for design. The calculated shear capacity of FCCC-Rs and the contribution of the three parts are listed in Table 8.

5. Conclusions

In this study, the shear behaviour of FCCC-Rs was investigated in three-point bending tests of 28 short specimens. Four parameters, i.e., the concrete strength, shear-span ratio, FRP tube thickness and fibre orientation, were experimentally investigated. Design equations for the shear strength of FCCC-Rs were proposed based on previous research as well as the test data obtained in this study. The following conclusions can be drawn:

(1) The majority of the FCCC-R specimens fail in the ductile mode, which indicates that the combination action of the FRP tube and high-strength steel bar can improve the ductility of the infilling concrete under shear;
(2) The failure mode is determined by the shear-span ratio (λ). The specimens with lower λ values tend to fail in shear. All specimens with $\lambda = 0.2$ fail in shear;
(3) The fibre orientation strongly influences the shear capacity of FCCC-Rs. It is suggested that inclined fibres should be designed for FRP tubes when the FCCC-R component is subjected to shear;
(4) The proposed design equations fit the test data well and are conservative in the high-strength region. The design equations are applicable for evaluation of the shear capacity of FCCC-R in composite structures

There are several questions of the shear properties of the FCCC-Rs need further investigation for future studies:

(1) This paper focuses on the shear behaviour of FCCC-R at the structural component level. In structural member level, the FCCC-

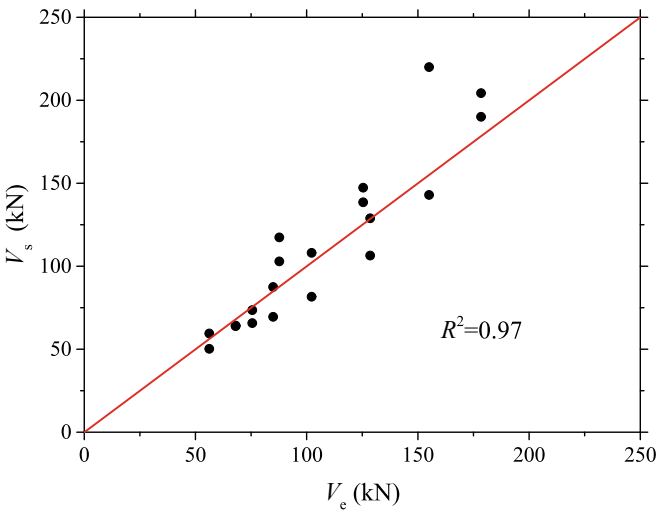

Fig. 12. Calculation results ($V_{cal.}$) and experimental results ($V_{exp.}$).

Table 8
Calculation results ($V_{cal.}$) and contribution of the three parts.

Specimens	Test results $V_{exp.}$ (kN)	Calculation results			
		V_f (kN)	v_s (kN)	V_c(kN)	$V_{cal.}$ (kN)
T3A85-C40R-0.5-1	63.91	28.14	22.37	17.57	68.08
T3A85-C40R-0.5-2	64.23				
T3A85-C60R-0.5-1	73.54	28.14	28.13	19.25	75.53
T3A85-C60R-0.5-2	65.77				
T3A85-UHPCR-0.5-1	106.45	28.14	60.96	39.42	128.52
T3A85-UHPCR-0.5-2	128.90				
T3A60-C60R-0.5-1	138.51	78.02	28.13	19.25	125.40
T3A60-C60R-0.5-2	147.35				
T3A60-UHPCR-0.5-1	190.04	78.02	60.96	39.42	178.40
T3A60-UHPCR-0.5-2	204.28				
T4A85-C60R-0.5-1	87.50	37.52	28.13	19.25	84.91
T4A85-C60R-0.5-2	69.50				
T3A85-C60R-1-1	50.27	17.32	19.66	19.25	56.23
T3A85-C60R-1-2	59.50				
T3A85-UHPCR-1-1	102.90	17.32	42.60	27.78	87.69
T3A85-UHPCR-1-2	117.39				
T3A85-C60R-0.2-1	81.66	45.03	37.95	19.25	102.23
T3A85-C60R-0.2-2	108.10				
T3A85-UHPCR-0.2-1	143.00	45.03	82.22	27.78	155.03
T3A85-UHPCR-0.2-2	220.00				

Rs contribute to the total shear capacity by the dowel action itself as well as the interaction with surrounding concrete and stirrups. It is important to quantify the contribution of FCCC-Rs in structural member level;

(2) This work tested the influence of shear-span ratio of the FCCC-R component. When subjected to shear in the composite member, the concrete cracks propagate inclined to the FCCC-R's axis. Therefore, the actual shear-span and the shear load direction need to be clarified;

(3) The FCCC-R components are to be used in the vertical structural members such as columns and shear walls, in which the FCCC-R will be subjected to combined axial compression and shear. The behaviour of this component under such loading case need to be studied in the future;

(4) The smaller fibre angle can lead to higher shear capacity but lower axial compression strength [7]. It is necessary to make a balance between these two aspects in structural design.

Data Availability Statement

All data, models, and code generated or used in this study are provided in the submitted article.

CRediT authorship contribution statement

Li Hu: Conceptualization, Methodology, Writing – original draft, Validation, Investigation, Data curation, Visualization. **Peng Feng:** Methodology, Writing – review & editing, Funding acquisition, Supervision. **Jia-Qi Yang:** Writing – review & editing. **Zhiyuan Li:** Writing – review & editing.

Declaration of Competing Interest

The authors declare that they have no known competing financial interests or personal relationships that could have appeared to influence the work reported in this paper.

Data availability

Data will be made available on request.

Acknowledgements

This work was supported by the National Natural Science Foundation of China (No. U2106219 and 51978379), and the Institute of Guo Qiang, Tsinghua University (No. 2019GQG1004 and 2021GQI0007).

References

[1] Lam L, Teng JG. Design-oriented stress– strain model for FRP-confined concrete. Constr Build Mater 2003;17(6-7):471–89.
[2] Jiang T, Teng JG. Analysis-oriented stress–strain models for FRP–confined concrete. Eng Struct 2007;29:2968–86.
[3] Ozbakkaloglu T, Lim JC. Axial compressive behavior of FRP-confined concrete: experimental test database and a new design-oriented model. Compos B Eng 2013;55:607–34.
[4] Samaan M, Mirmiran A, Shahawy M. Model of concrete confined by fiber composites. J Struct Eng-ASCE 1998;124(9):1025–31.
[5] Yang J, Feng P. Analysis-oriented models for FRP-confined concrete: 3D interpretation and general methodology. Eng Struct 2020;216:110749.
[6] Yang J, Feng P. Analysis-oriented model for FRP confined high-strength concrete: 3D interpretation of path dependency. Compos Struct 2021;278:114695.
[7] Li Z, Feng P, Yang JQ. Analysis-oriented model for FRP tube-confined concrete: 3D interpretation of biaxial tube behaviour. Eng Struct 2022;272:114987.
[8] Feng P, Cheng S, Bai Y, Ye L. Mechanical behavior of concrete-filled square steel tube with FRP-confined concrete core subjected to axial compression. Compos Struct 2015;123:312–24.
[9] Feng P, Cheng S, Yu T. Seismic performance of hybrid columns of concrete-filled square steel tube with FRP-confined concrete core. J Compos Constr 2018;22(4):04018015.
[10] Teng J, Wang Z, Yu T, Zhao Y, Li LJ. Double-tube concrete columns with a high-strength internal steel tube: Concept and behaviour under axial compression. Adv Struct Eng 2018;21. 136943321774683.
[11] Fardis MN, Khalili H. Concrete encased in fiber glass-reinforced plastic. J Am Concr Inst 1981;78(6):440–6.
[12] Wang J, Feng P, Hao T, Yue Q. Axial compressive behavior of seawater coral aggregate concrete-filled FRP tubes. Constr Build Mater 2017;147:272–85.
[13] Wang Z. RC columns reinforced with FCCC-R: axial compressive behavior and seismic performance. Beijing, China, Tsinghua University. Doctoral Dissertation; 2018.
[14] Wang Z, Feng P, Zhao Y, Yu T. FRP-confined concrete core-encased rebar for RC columns: Concept and axial compressive behavior. Compos Struct 2019;222:110915.
[15] Wang Z, Li Z, Feng P. Cyclic axial compressive performance of the RC columns reinforced with FRP confined concrete core encased rebar. Eng Struct 2022;274:115166.
[16] Hu L, Feng P, Lin H, Yang JQ, Qiang H. Seismic performance of composite shear walls with embedded FCCCs in boundary elements. Compos Struct 2020;257:113126.
[17] Hu L. Study on seismic performance of RC shear walls with embedded FCCCs. Beijing, China, Tsinghua University. Doctoral Dissertation; 2021.
[18] Seible F, Priestley MJN, Hegemier GA, Innamorato D. Seismic retrofit of RC columns with continuous carbon fiber jackets. J Compos Constr – ASCE 1997;1(2):52–62.
[19] Bhide KM. Shear response of concrete filled circular fiber-reinforced-polymer composite tubes. Ann Arbor, Michigan State University. Master's thesis; 1998.
[20] Davol A. Mechanical characterization of concrete filled FRP members. La Joll, California, University of California, San Diego. Doctoral Dissertation; 1998.
[21] Burgueño R. System characterization, and design of modular fiber reinforced polymer (FRP) short and medium-span bridges. La Jolla, California, University of California, San Diego. Doctoral Dissertation; 1999.
[22] Burgueño R, Bhide K. Shear behavior of concrete filled circular FRP tubes. In: Conference: Structures Congress, 2004; 2004.
[23] Burgueño R, Bhide K. Shear response of concrete-filled FRP Composite cylindrical shells. J Struct Eng-ASCE 2006;132(6):940–60.

[24] Ahmad I. Shear response and bending fatigue behavior of concrete-filled fiber reinforced polymer tubes. Raleigh, North Carolina State University. Doctoral Dissertation; 2004.
[25] Ahmad I, Zhu Z, Mirmiran A. Behavior of short and deep beams made of concrete-filled fiber-reinforced polymer tubes. J Compos Constr 2008;12(1):102–10.
[26] Fam A, Cole B. Tests on reinforced-concrete-filled, fiber-reinforced-polymer circular tubes of different shear spans. Can J Civ Eng 2007;34(3):311–22.
[27] Shi Y, Li B, Mirmiran A. Combined shear and flexural behavior of hybrid FRP-concrete beams previously subjected to cyclic loading. J Compos Constr – ASCE 2011;15(5):841–9.
[28] Zhang B, Hu XM, Zhao Q, Huang T, Zhang NY, Zhang Q-B. Effect of fiber angles on normal- and high-strength concrete-filled fiber-reinforced polymer tubes under monotonic axial compression. Adv Struct Eng 2020;23(5):924–40.
[29] MOHURD. Technical code for infrastructure application of FRP composites. GB50608-2010. Beijing, China: Ministry of Housing and Urban-Rural Development (MOHURD) of People's Republic of China; 2010 [In Chinese].
[30] MOHURD. Code for design of concrete structures. GB50010-2010. Beijing, China: Ministry of Housing and Urban-Rural Development (MOHURD) of People's Republic of China; 2010 [In Chinese].
[31] Lv X, Wang Y, Fu C, Zheng W. Basic mechanical property indexes of reactive powder concrete. J Harbin Inst Technol 2014;46:1–9.
[32] ASTM. Standard test method for apparent hoop tensile strength of plastic or reinforced plastic pipe by split disk method. ASTM D2290-12. West Conshohocken, PA. American Society of Testing Materials, ASTM; 2012.
[33] Vintzeleou EN, Tassios TP. Behavior of dowels under cyclic deformations. ACI Struct J 1987;84:18–30.